Measuring the impact of spin-triplet exciton orientation on photocurrent in an organic transistor

Journal:	*Journal of Materials Chemistry C*
Manuscript ID	TC-ART-04-2021-001539.R1
Article Type:	Paper
Date Submitted by the Author:	04-Jun-2021
Complete List of Authors:	Bittle, Emily; National Institute of Standards and Technology, Engmann, Sebastian; NIST, ; Theiss Research, Thorley, Karl; University of Kentucky, Chemistry Anthony, John; University of Kentucky, Chemistry and Advanced Carbon Materials

Measuring the impact of spin-triplet exciton orientation on photocurrent in an organic transistor

Submitting to: Journal of Materials Chemistry C (EI)

Emily G. Bittle[1], Sebastian Engmann[1,2], Karl Thorley[3], John Anthony[3]

Abstract: The dynamics of triplet and singlet exciton populations in organic semiconductors offer interesting possibilities in improving optical device efficiency, while also attracting interest for future applications as manipulable states for quantum-state based computing. For technological applications, transduction of the exciton state is essential, thus detailed information on how the exciton dynamics affect device outputs is required. In this study, we measure the magnetic field response of the photocurrent in organic transistors to investigate the electrical signal resulting from singlet-triplet exciton dynamics. We find that controlling the orientation of the magnetic dipole orientation of the triplet by varying both the magnitude and orientation of the magnetic field with respect to single crystal axes in *anti*-2,8-difluoro-5,11-bis(triethylsilylethynyl)anthradithiophene (*a*diF TES ADT), allows us to manipulate the amount of current detected as a result of singlet fission.

[1]Nanoscale Device Characterization Division, National Institute of Standards and Technology,
101 Bureau Drive, Gaithersburg, Maryland, 20899, United States

[2]Theiss Research, La Jolla, California 92037, United States

[3]Department of Chemistry, University of Kentucky, Lexington, Kentucky 40506, USA

Organic semiconductors support long lived excitons at room temperature due to a high binding energy resulting from the low dielectric constant in these materials[1]. In certain organic semiconductors optically-excited singlet-state excitons can spontaneously decay to the triplet state. In the process of singlet fission, a singlet exciton produces two triplet excitons. Triplet excitons then have a prolonged lifetime due to their spin-forbidden transition to the ground state and can live for microseconds[2]. Spontaneous singlet fission/triplet fusion has been studied for many years in organic materials and has gained attention as a way to increase efficiency in organic light emitting diodes (LEDs) and photovoltaics.[3] While singlet fission can be observed in ultrafast optical[4] and electron spin resonance experiments[5], quantifying the impact of this process on devices is complicated by electrical interfaces, electrostatics, and slow response of the device when compared to exciton lifetimes. For example, "low voltage turn-on" has been suggested as a signature of triplet fusion driving device enhancement in OLEDs[6–10], though we recently have shown that the heterojunction band-offset in OLEDs is likely to drive this behavior.[11] This leads to further questions about the impact that spontaneous fission/fusion has on the enhancement of devices. Therefore, device based experiments are required to develop better diagnostics of the impact of exciton processes on device performance.

In addition to the improvement of traditional devices, unique exciton states are being investigated for their possible use in future computing paradigms.[12,13] Especially enticing are ways to move complex novel computing from low temperature into room temperature systems. This requires the relevant quantum state to have a larger energy than the surrounding environment. Excitons in organic semiconductors routinely have binding energies that are well above $k_B T$ at room temperature[3] resulting in longer lifetimes compared with traditional inorganic excitons, and singlet fission/triplet fusion demonstrate unique processes that can be used to manipulate available exciton states[14,15]. The control of singlet and triplet populations made possible through spontaneous singlet fission via a coherent triplet pair state can be exploited for applications in magnetic field sensing or can be further refined to produce quantum states useful for calculation.

Our previous study of magneto-photocurrent in tetracene showed that there is a dependence of the magnetic field response depending on the in-plane orientation of the tetracene crystal with respect to the magnetic field.[16] In this study, we refine the measurement and calculation and apply the technique to single crystals of *anti*- 2,8-difluoro-5,11-bis(triethylsilylethynyl)anthradithiophene (*a*diF TES ADT)[17]. In tetracene crystals, the herringbone molecular configuration puts molecules, and thereby magnetic axes, at nearly perpendicular arrangement on the flat plane of the crystal. Molecules in *a*diF TES ADT crystals arrange relatively parallel in the large area *ab* plane[18] which will also align the magnetic dipoles of neighboring molecules in the crystal.

We look at the impact that singlet fission has on the output current of a transistor in a magnetic field as a function of crystal orientation. We correlate changes in the magnetic field response of the photocurrent with crystal orientation to calculations of singlet fission based on a simple spin Hamiltonian. From this, we gain insight into the steady state population density changes of singlet and triplet states. The result reflects the spin character of the triplets formed by singlet fission and is highly influenced by the zero-field splitting caused by the magnetic dipole-dipole interaction within the triplet exciton for fields in the range of 0 mT to 200 mT. Using the transistor as an electrical probe of the exciton population shows the possibility to transduce exciton signal into solid state electrical systems and allows for single-crystal device studies which provide a platform for understanding physics in ordered systems[19] and exploiting anisotropic effects[20].

Experimental:

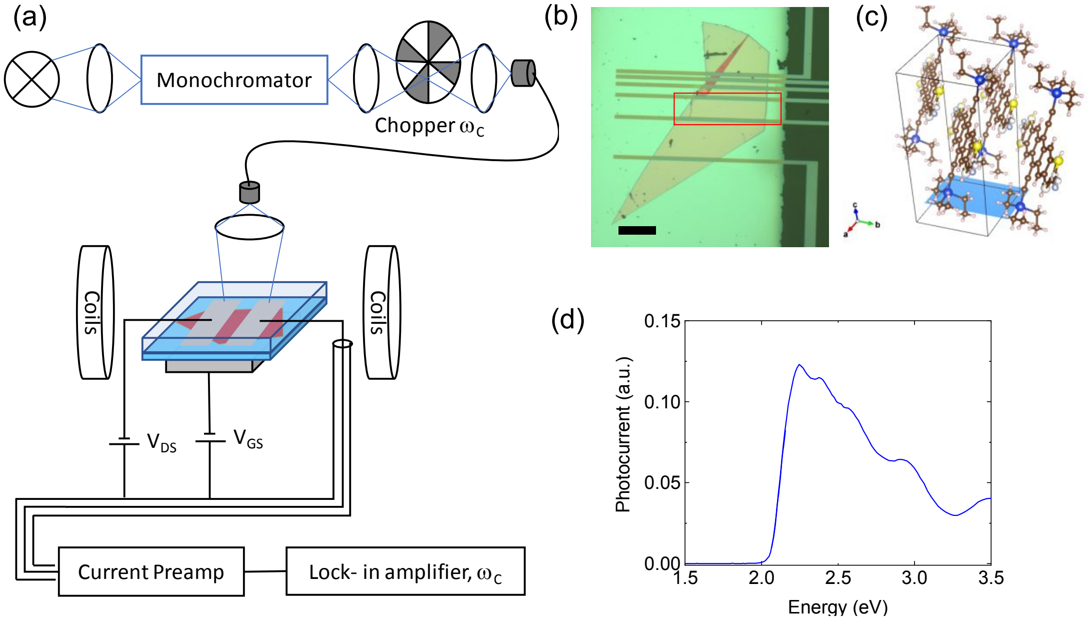

Figure 1: (a) Diagram of the measurement. The sample was placed between the coils of an electromagnet and was illuminated with light from a monochromator (blue lines follow the path of the light). Signal was measured at chopping frequency $\omega_C = 327$ Hz. (b) Micrograph of the sample used for the main paper. The pinkish-orange shape is a single crystal of *a*diF TES ADT. The yellow area is the gate metal and horizontal darker yellow thin lines are drain/source contacts with varying distances. The 50 μm long channel was used for MPC measurements, outlined by the red box. Black scale bar shows 100 μm. (c) Structure of *a*diF TES ADT[21,22]. The drain-source plane of the crystal in the measured transistor lies near the *ab* plane.[18] (d) Photocurrent spectrum of *a*diF TES ADT with no magnetic field, gate-source voltage set to -10 V and drain-source voltage set to -1 V.

A simplified representation of the measurement set-up is shown in Figure 1a. Transistors were made in top gate bottom contact configuration on quartz substrates to allow optical access from the bottom of the sample, the transistor used for this study is shown in Figure 1b. Drain and source contacts are masked using optical lithography; Au or Pd was thermally evaporated and treated to produce a self-assembled monolayer of pentafluorobenzenethiol to improve contact resistance.[23] Semiconductor crystals were grown using physical vapor growth[24,25] in quartz tubes, with the source material temperature at 160 °C, argon gas flow at 80 cm^3 60 s^{-1} for seven days to achieve crystals ≈ 0.5 mm on a side in the *ab*-plane. Crystals were hand positioned using a hair from a synthetic paint brush and electrostatically held to the sample substrate and contacts. Polymer dielectric Teflon was applied using spin coating (at 500 ($2\pi/60$) rad s^{-1} for 5 s and 3000 ($2\pi/60$) rad s^{-1} for 45 s), dried for 2 h in a nitrogen purge box and then further dried overnight in vacuum at room temperature. Teflon AF 2400 was dissolved in a 25 mg/mL solution with Fluorinert FC-40 at 60 °C for five days before coating.[26] Capacitance per area C/A $= 1.15\times10^{-4}$ F/m^2 was measured, which corresponds to approximate dielectric thickness of 150 nm. Aluminum was used as the gate metal and was evaporated through a shadow mask. Current-voltage characteristics of the transistor used to produce data in the main text are shown in Supplementary Material, figure S1.

The sample is illuminated though the glass substrate with monochromatic light chopped at 327 Hz. The transistor gate and drain are held at constant bias using two matching battery sources with common ground. Photocurrent through the source contact is measured through a preamplifier set to 1 μA/V with a 6 dB bandpass filter set to cutoff at 3 Hz and 3 kHz. The signal is processed using a lock-in amplifier set to the optical chopper frequency with time constant at 300 ms. To obtain magnetic field dependence of the photocurrent, an electromagnet is used to incrementally step the magnetic field, which is measured between the poles using a Hall bar sensor with 7.78×10^{-2} V/T sensitivity. The sample is mounted on a manual rotation stage with 1-degree accuracy to facilitate angle dependent measurements. The measurement is performed in a nitrogen purged glovebox.

Photocurrent at zero applied magnetic field as a function of wavelength is shown in figure 1d and agrees well with a previous study of photocurrent in diF TES ADT.[27] For measurements of photocurrent, the gate source voltage (V_{GS}) was set to -10 V and the drain-source voltage (V_{DS}) was set to -1 V (see Supplementary Material, figure S1). The photocurrent is zero below the singlet excitation energy around 2.1 eV, indicating that the photocurrent originates from the formation of a singlet exciton.

Results and Discussion:

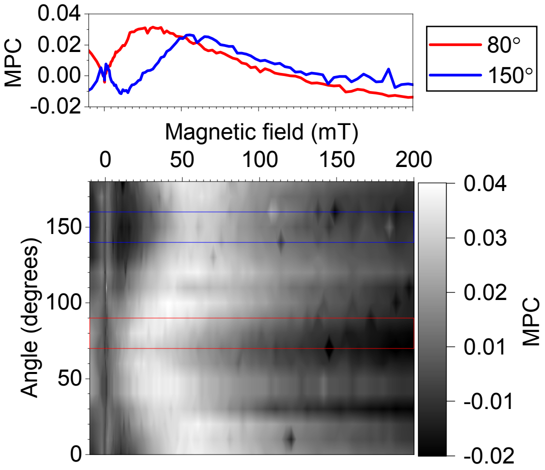

Figure 2: Magnetic field dependence of the photocurrent response in single crystal *a*diF TES ADT transistor. The magnetic field runs approximately parallel to the *ab* crystal plane. Photocurrent was produced using 550 nm light.

To investigate spin dependent processes in the photocurrent (I_p) owing to the spontaneous formation of triplets, the magnetic field was scanned between -10 mT and 200 mT to measure the magnetic-field effects on the photocurrent (MPC). MPC is expressed as relative photocurrent defined with respect to the zero-field photocurrent, MPC = [I_p (B) – I_p (B = 0 mT)] / I_p (B = 0 mT). The transistor was rotated from 0° to 180° in 10° steps. The magnetic field dependence of the photocurrent is shown in figure 2 and Supplementary Material figure S2 for a sample with Au contacts, and in figure S3 for a sample with Pd contacts. Similar signal was found for both samples (with crystals at different orientation with respect to the samples holder) suggesting that effects at the contacts do not contribute substantially to the signal. A broad peak can be observed shifting between 28 mT to 58 mT with orientation in the magnetic field. A narrow peak is seen below 10 mT at certain angles with a peak that shifts between 1.5 mT and 4 mT.

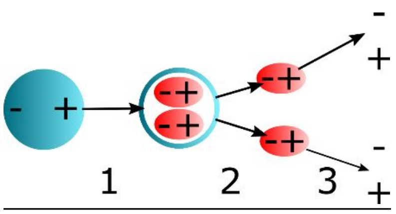

Figure 3: A simple diagram of singlet fission and triplet conversion to charges. In step 1, the singlet exciton (green, circle) spontaneously forms two bound triplet excitons (red, oval) with overall singlet character. In step 2 the triplet excitons separate into two independent quasi-particles which later decay into free charges (step 3).

To better understand the origin of the MPC, a simple model was used to calculate the photocurrent as a function of magnetic field amplitude and direction. A simple illustration of singlet fission to charge formation is shown in Figure 3. Due to the short lifetime and strong photoluminescence of the singlet state and relatively long lifetime and spin forbidden photoluminescence of the triplet[28], we assume that all singlet excitons will either decay to the ground state without contributing to the photocurrent or will go through singlet fission to form triplets which then decay to free charges. Triplet decay to charges can happen when the local electric field is high enough to overcome the binding energy, which is possible in transistors at the metal contact[23,29], due to gate field, or when interacting with radical or trap states.[27,30–32]

We determine the density of triplet state excitons and resulting photocurrent through singlet fission using a model developed by Timmel et al.[33] that we previously applied to understand anisotropic MPC in tetracene.[16] At steady state (relevant to our slow measurements at 327 Hz) the triplet population is

$$\Phi_T(B) = 1 - \sum_{m,n} \left|P^{S}_{mn}\right|^2 \frac{\mathrm{k}^2}{\mathrm{k}^2 + (\omega_\mathrm{m} - \omega_\mathrm{n})^2} \qquad \text{Equation 1}$$

The triplet-triplet pair states formed (m and n) by spontaneous singlet fission will match the spin character of the singlet state S, such that the quantum probability $P^{S}_{mn} = \langle m|S\rangle\langle S|n\rangle$, where <S|m> is the overlap in singlet and triplet-triplet pair states, will be non-zero. The energy of the triplet state is given by $E_l = \hbar\omega_l$ and we assume that the formation rate k has one value. The calculated magneto-photocurrent is proportional to the triplet density in a magnetic field normalized to the triplet density with no field:

$$MPC \propto \frac{\Phi_T(B) - \Phi_T(0)}{\Phi_T(0)} \qquad \text{Equation 2}$$

The two interacting triplets were modelled using a simple spin Hamiltonian

$$H = \sum_{i=1}^{2}(H_{Zi} + H_{Ti}) + H_{ex} \quad \text{Equation 3}$$

Where H_{Zi} is the Zeeman interaction

$$H_{Zi} = \mu_B g_i \vec{S}^i \cdot \vec{B} \qquad \text{Equation 4}$$

μ_B is the Bohr magneton, the g-factor is set to 2, S^i is the spin operator of spin *i*, and B is the magnetic field. The zero-field splitting (H_{Ti}) due to unpaired spin interactions is given by

$$H_{Ti} = \frac{1}{3}D\left((S_z^i)^2 - S^i(S^i + 1)\right) + E\left((S_x^{\mathrm{i}})^2 + (S_y^i)^2\right) \quad \text{Equation 5}$$

Where D and E are experimentally determined values of the zero field splitting parameters in the molecular crystal, which originate in the spin-spin interactions of charges within an exciton. When comparing the model to the single crystal data, an arbitrary offset is required as the orientation of the D/E frame is not regularly measured in experiments using polycrystalline samples[28,34]. The exchange interaction for two spins *i* and *j*

$$H_{ex} = -J\left(\left(\vec{S}^i \cdot \vec{S}^j\right) + {}^{1}/_{4}\right) \qquad \text{Equation 6}$$

Where we have used $J \approx 1.24 \times 10^{-2}$ μeV (<< D).[31]

To calculate the energy levels and eigenvalues of the nine triplet pair states, we use EasySpin written by Stoll and Schweiger[35] and solve for a system of two spin 1 particles. The relevant singlet state is derived from previous work[36] and we give a brief description here. A four-electron system will result in two states with overall spin S = 0. One is a combination of two singlet states and the other can be represented in the zero-field triplet state basis giving a spin allowed singlet state that has significant triplet character. This state, defined in the diagonalized zero-field triplet basis with the triplet states |x>, |y> and |z>, is given by

$$|S\rangle = \frac{1}{\sqrt{3}}(|x\rangle|x\rangle + |y\rangle|y\rangle + |z\rangle|z\rangle) \quad \text{Equation 7}$$

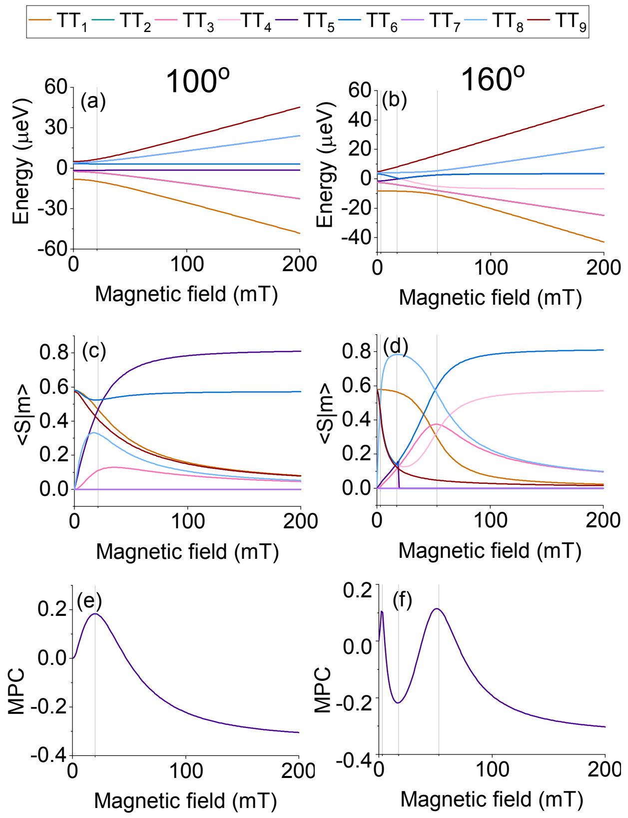

Figure 4 Results of calculation for triplet pair energy, singlet-triplet pair state overlap and magneto-photocurrent at 100° and 160°. Triplet levels are labelled from lowest to highest energy, with energy differences defined with respect to the B = 0 triplet energy without zero-field splitting. Grey lines indicate inflection points in the MPC. (a), (c), and (e) show 100°; (b), (d), and (f) show 160°, which are defined with respect to the magnetic axes as defined by the Hamiltonian given in Equation 3.

The triplet pair energy and eigenstate overlap with the singlet are both affected by the magnetic field, as shown in Figure 4 for two orientations of the crystal in the magnetic field. TT_i indicates the nine triplet-triplet pairs (eigenstates calculated from Equation (3)) and are ordered from $i = 0$ to $i = 9$ from lowest to highest energy. The calculated MPC is also shown. So long as k is smaller than the energy difference, $k < \omega_m - \omega_n \approx 1\ \mathrm{ns}^{-1}$, we get a result that agrees well with experiment.[16,33] Peaks and valleys in the resulting MPC most closely follow the overall singlet character of the triplet states. As seen in Figure 4 (e), the one inflection point marked with a grey vertical line in the MPC occurs at a crossing point in the singlet character of the various TT states in (c). Similarly, the three inflection points in (f) correlate with crossover in singlet character between TT states in Figure 4 (d). These crossover points coincide with avoided crossings in the energy spectrums Figure 4 (a) and (b).

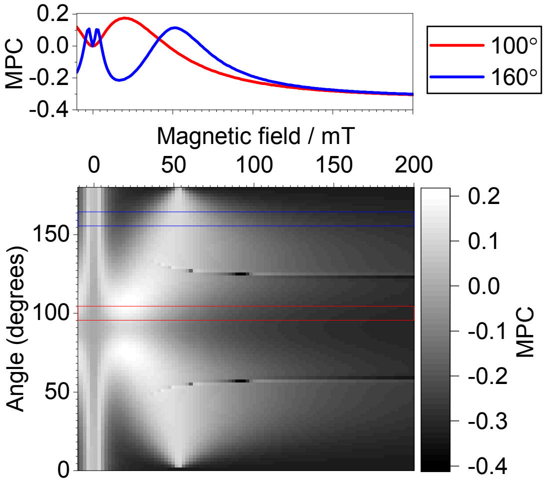

Figure 5 Results of the magneto-photocurrent calculation. The top graph shows line profiles of the average of regions marked in red and blue on the bottom graph centered at 100° and 160°. Avoided crossings in the energy levels produce sharp changes in the MPC, seen around 50° and 125° in the calculation. These sharp changes will not be observable in the reported experiment.

A plot of the results of the photocurrent calculation for magnetic field amplitude and direction is shown in Figure 5. The position of the peaks and valleys in the MPC with respect to magnetic field and orientation are affected by the values for D and E in the zero-field splitting term, as these values determine the energetic spread of the B = 0 T energies of the triplet-triplet states and therefore the magnetic field values of avoided crossings as energies change linearly as a result of the Zeeman effect (Equation (4)). In comparison to the experimental results shown in Figure 2, a best estimate gives D = 6.2 μeV and E = 0.4 μeV. These values are in reasonable agreement to results from optically detected magneto-resonance measurements done on diF TES ADT: D = 5.38 μeV and E =0.12 μeV[28]. It should be noted that the D and E values of the triplet state given here are measured in a crystal. With a phase transition near room temperature, diF TES ADT can exhibit multiple phases at room temperature[37] which may contribute to differences in the dipolar interaction terms when comparing studies. Due to the geometry and processing of the device, we are not able to determine the exact crystal structure for the single crystal reported here.

For *a*diF TES ADT in the magnetic field range of 0 mT to 200 mT, we find that the qualitative shape of the magneto-photocurrent can be modelled by the spontaneous formation of triplet states from photogenerated singlet states. Depending on magnitude and orientation, we can control spontaneous fission and detect the resulting current in a device that is simple to fabricate. Matching the model and experiment, we get an approximately 75° offset between the device holder axes and the axes defined by the zero-field splitting parameters. Previous studies of magneto-electroluminescence have used hyperfine interactions between polaron pairs to describe behavior below 500 μT.[38] As the fields measured here are well above the approximate local hyperfine fields for polarons, our results agree well with previous studies which do not take into account the hyperfine term.[28,39] Photocurrent in single crystals of tetracene similarly shows a structured, anisotropic magnetic field response for fields 0 mT to 200 mT[16] and between 200 mT and 500 mT[40] that can be well described by a model including the zero-field splitting of the triplet exciton.

Key differences between the modelled data and experiment may reflect the simplifications in the model where the device properties are not considered. For example, the magnitude of the resulting change in photocurrent is much larger in the model compared to experiment. This may be due to simplifying assumptions in which singlet excitons do not contribute to current, or to assumptions regarding the collection of charges from triplet states. We have built a device that supports majority hole transport using high work function drain and source contacts with a material that typically works as a p-type-like semiconductor. The result is that there are not efficient pathways for negative charges to escape the device. The free negative charges may then recombine with free holes, decreasing the carriers that can contribute to current in the device. Similarly, this effect may result in the positive offset of values in the experiment when compared to the model, as a lower triplet formation will also result in a smaller number of these free electrons formed. Furthermore, real device defect density and crystal structure affect both charge transport and exciton dynamics[41,42], resulting in changes to expected results. These cases illustrate the importance of device design in balancing competing effects that can decrease the device enhancements predicted from ultra-fast optical measurements of exciton dynamics and impact the accurate measurement of exciton population dynamics on devices.

The possibilities of using singlet-triplet exciton dynamic states for enhancement of device efficiency and computation have been driven by observations from ultra-fast optical measurements and electron spin resonance measurements. While these measurements show intriguing physics, current indicator measurements of the impact of triplet/singlet interconversion in devices do not easily, quantitatively, and unambiguously show the improvements made through synthesis of new molecules/polymers or through device design.[11] Unambiguously determining the effect of triplet/singlet interconversion in device measurements is difficult due to the slow response (≈ MHz in diodes) [43] and size of devices (> 10's nm) compared to exciton lifetimes (GHz) and diffusion lengths (<10's nm)[1]. Further work on triplet/singlet exciton dynamics in organic semiconductor devices should therefore pursue an indicator metric which

1) Shows true indication of triplet enhanced performance of devices
2) Quantifies the changes in device performance that are due to singlet/triplet interconversion
3) Is easy to use to encourage universal acceptance

Developing an indicator metric will take coordination between device and ultra-fast physical measurements. The metric would allow for the progressive development of materials and device structures that take advantage of singlet/triplet interconversion.

Conclusion:

In this paper, we demonstrate a relatively simple indicator measurement of changes to photocurrent signal when directly manipulating the triplet/singlet dynamics using a magnetic field. We've shown that the measurement and model presented here indicate singlet/triplet interconversion in *a*diF TES ADT. Our goal in future studies is to develop methods to quantify the impact of singlet/triplet exciton dynamics on completed device structures using the magnetic field response of devices.

Author Contributions:

E.G.B. designed the experiment, collected data, performed calculations, and wrote the manuscript. S.E. assisted in experiment design and calculations. K.T. and J. A. synthesized the *a*diF TES ADT. All authors reviewed and edited the final manuscript.

Conflicts of interest:

There are no conflicts to declare.

Acknowledgements:

The authors thank Elise Treat and David Rutter for assistance on experimental design. S.E. acknowledges support from the U.S. Department of Commerce, National Institute of Standards and Technology under the financial assistance award 70NANB17H305. JA and KT acknowledge support from the US National Science Foundation, under Cooperative Agreement No. 1849213. Certain commercial equipment, instruments, or materials are identified in this paper in order to specify the experimental procedure adequately. Such identification is not intended to imply recommendation or endorsement by the National Institute of Standards and Technology, nor is it intended to imply that the materials or equipment identified are necessarily the best available for the purpose.

References:

1 C. J. Bardeen, *Annu. Rev. Phys. Chem.*, 2014, **65**, 127–148.

2 A. B. Pun, A. Asadpoordarvish, E. Kumarasamy, M. J. Y. Tayebjee, D. Niesner, D. R. McCamey, S. N. Sanders, L. M. Campos and M. Y. Sfeir, *Nat. Chem.*, 2019, **11**, 821–828.

3 A. Köhler and H. Bässler, *Mater. Sci. Eng. R Reports*, 2009, **66**, 71–109.

4 C. D. Cruz, E. L. Chronister and C. J. Bardeen, *J. Chem. Phys.*, 2020, **153**, 234504.

5 L. R. Weiss, S. L. Bayliss, F. Kraffert, K. J. Thorley, J. E. Anthony, R. Bittl, R. H. Friend, A. Rao, N. C. Greenham and J. Behrends, *Nat. Phys.*, 2017, **13**, 176–181.

6 A. K. Pandey and J. M. Nunzi, *Appl. Phys. Lett.*, 2007, **90**, 263508.

7 S.-J. He and Z.-H. Lu, *J. Photonics Energy*, 2016, **6**, 036001.

8 C. Xiang, C. Peng, Y. Chen and F. So, *Small*, 2015, **11**, 5439–5443.

9 Q. Chen, W. Jia, L. Chen, D. Yuan, Y. Zou and Z. Xiong, *Sci. Rep.*, 2016, **6**, 1–9.

10 A. K. Pandey, *Sci. Rep.*, 2015, **5**, 1–6.

11 S. Engmann, A. J. Barito, E. G. Bittle, N. C. Giebink, L. J. Richter and D. J. Gundlach, *Nat. Commun.*, 2019, **10**, 227.

12 N. Y. Kim and Y. Yamamoto, *Exciton-Polariton Quantum Simulators*, Springer, Cham, 2017.

13 C. J. Bardeen, *J. Chem. Phys.*, 2019, **151**, 124503.

14 J. J. Burdett and C. J. Bardeen, *J. Am. Chem. Soc.*, 2012, **134**, 8597–8607.

15 S. L. Bayliss, L. R. Weiss, A. Rao, R. H. Friend, A. D. Chepelianskii and N. C. Greenham, *Phys. Rev. B*, 2016, **94**, 45204.

16 H. J. Jang, E. G. Bittle, Q. Zhang, A. J. Biacchi, C. A. Richter and D. J. Gundlach, *ACS Nano*, 2019, **13**, 616–623.

17 P. J. Diemer, J. Hayes, E. Welchman, R. Hallani, S. J. Pookpanratana, C. A. Hacker, C. A. Richter, J. E. Anthony, T. Thonhauser and O. D. Jurchescu, *Adv. Electron. Mater.*, 2017, **3**, 1600294.

18 O. D. Jurchescu, S. Subramanian, R. J. Kline, S. D. Hudson, J. E. Anthony, T. N. Jackson and D. J. Gundlach, *Chem. Mater.*, 2008, **20**, 6733–6737.

19 V. Podzorov, *MRS Bull.*, 2013, **38**, 15–24.

20 E. G. Bittle, A. J. Biacchi, L. A. Fredin, A. A. Herzing, T. C. Allison, A. R. Hight Walker and D. J. Gundlach, *Commun. Phys.*, 2019, **2**, 29.

21 R. K. Hallani, K. J. Thorley, Y. Mei, S. R. Parkin, O. D. Jurchescu and J. E. Anthony, *Adv. Funct. Mater.*, 2016, **26**, 2341–2348.

22 K. Momma and F. Izumi, *J. Appl. Crystallogr.*, 2011, **44**, 1272–1276.

23 M. Waldrip, O. D. O. D. Jurchescu, D. J. D. J. Gundlach and E. G. E. G. Bittle, *Adv.*

Funct. Mater., 2020, **30**, 1904576.

24 R. . Laudise, C. Kloc, P. . Simpkins and T. Siegrist, *J. Cryst. Growth*, 1998, **187**, 449–454.

25 C. Kloc, P. G. Simpkins, T. Siegrist and R. A. Laudise, *J. Cryst. Growth*, 1997, **182**, 416–427.

26 A. F. Paterson, A. D. Mottram, H. Faber, M. R. Niazi, Z. Fei, M. Heeney and T. D. Anthopoulos, *Adv. Electron. Mater.*, 2019, **5**, 1800723.

27 K. Paudel, G. Giesbers, J. Van Schenck, J. E. Anthony and O. Ostroverkhova, *Org. Electron.*, 2019, **67**, 311–319.

28 C. K. Yong, A. J. Musser, S. L. Bayliss, S. Lukman, H. Tamura, O. Bubnova, R. K. Hallani, A. Meneau, R. Resel, M. Maruyama, S. Hotta, L. M. Herz, D. Beljonne, J. E. Anthony, J. Clark and H. Sirringhaus, *Nat. Commun.*, 2017, **8**, 15953.

29 J. Day, A. D. Platt, S. Subramanian, J. E. Anthony and O. Ostroverkhova, *J. Appl. Phys.*, 2009, **105**, 103703.

30 B. T. Lim, J. Cho, K. H. Cheon, K. Shin and D. S. Chung, *Org. Electron.*, 2015, **18**, 113–117.

31 R. E. Merrifield, *Pure Appl. Chem.*, 1971, **27**, 481–498.

32 C. Liewald, D. Reiser, C. Westermeier and B. Nickel, *Appl. Phys. Lett.*, 2016, **109**, 053301.

33 C. R. Timmel, U. Till, B. Brocklehurst, K. A. McLauchlan and P. J. Hore, *Mol. Phys.*, 1998, **95**, 71–89.

34 S. L. Bayliss, A. D. Chepelianskii, A. Sepe, B. J. Walker, B. Ehrler, M. J. Bruzek, J. E. Anthony and N. C. Greenham, *Phys. Rev. Lett.*, 2014, **112**, 238701.

35 S. Stoll and A. Schweiger, *J. Magn. Reson.*, 2006, **178**, 42–55.

36 J. J. Burdett, G. B. Piland and C. J. Bardeen, *Chem. Phys. Lett.*, 2013, **585**, 1–10.

37 O. D. Jurchescu, D. A. Mourey, S. Subramanian, S. R. Parkin, B. M. Vogel, J. E. Anthony, T. N. Jackson and D. J. Gundlach, *Phys. Rev. B - Condens. Matter Mater. Phys.*,

2009, **80**, 085201.

38 Z. Weng, W. P. Gillin and T. Kreouzis, Fitting the magnetoresponses of the OLED using polaron pair model to obtain spin-pair dynamics and local hyperfine fields, moz-extension://fa29bd03-24d6-419e-917b-daab7b8af701/enhanced-reader.html?openApp&pdf=https%3A%2F%2Fwww.nature.com%2Farticles%2Fs41598-020-73953-w.pdf, (accessed 19 May 2021).

39 G. B. Piland, J. J. Burdett, D. Kurunthu and C. J. Bardeen, *J. Phys. Chem. C*, 2013, **117**, 1224–1236.

40 N. E. Geacintov, M. Pope and S. Fox, *J. Phys. Chem. Solids*, 1970, **31**, 1375–1379.

41 P. Irkhin, I. Biaggio, T. Zimmerling, M. Döbeli and B. Batlogg, *Appl. Phys. Lett.*, 2016, **108**, 063302.

42 A. C. Jones, N. M. Kearns, J. J. Ho, J. T. Flach and M. T. Zanni, *Nat. Chem.*, 2020, **12**, 40–47.

43 L. C. C. Elliott, J. I. Basham, K. P. Pernstich, P. R. Shrestha, L. J. Richter, D. M. DeLongchamp and D. J. Gundlach, *Adv. Energy Mater.*, 2014, **4**, 1–8.